

Article

A Theoretical Analysis of Magnetic Particle Alignment in External Magnetic Fields Affected by Viscosity and Brownian Motion

Andrej Krafcik ^{1,*}, Peter Babinec ², Oliver Strbak ³ and Ivan Frollo ¹

¹ Department of Imaging Methods, Institute of Measurement Science, Slovak Academy of Sciences, Dubravska Cesta 9, 841 04 Bratislava, Slovakia; ivan.frollo@savba.sk

² Department of Nuclear Physics and Biophysics, Faculty of Mathematics, Physics and Informatics, Comenius University, Mlynska Dolina F1, 842 48 Bratislava, Slovakia; babinec@fmph.uniba.sk

³ Biomedical Center Martin, Jessenius Faculty of Medicine in Martin, Comenius University in Bratislava, Mala Hora 4, 036 01 Martin, Slovakia; oliver.strbak@centrum.cz

* Correspondence: andrej.krafcik@savba.sk

Featured Application: Iron oxide nanoparticles with highly nonlinear magnetic behavior are attractive for biomedical applications, including biosensing using the rotational freedom of particles for detection of biomarkers for cancer cells and for contrast enhancement in magnetic resonance imaging (MRI). Hyperthermia therapy has been used for cancer therapy, and magnetic particle imaging (MPI) is a promising new imaging modality that can spatially resolve the concentration of nanoparticles. For the success of the technology, understanding the nanoparticle rotation mechanism is necessary. The presented computational model can be used in the study of magnetic particle alignment phenomena as the non-Markovian process with memory in the external force field as part of generalized Langevin theory. It can elucidate the significance of each kind of torque in this phenomenon, or can serve as the estimator of the characteristic time of magnetic particle alignment in a wide range of magnitudes of the external magnetic flux density field. Our results, therefore, have far-reaching implications for understanding and advancement of these emerging biomedical technologies.

Abstract: The interaction of an external magnetic field with magnetic objects affects their response and is a fundamental property for many biomedical applications, including magnetic resonance and particle imaging, electromagnetic hyperthermia, and magnetic targeting and separation. Magnetic alignment and relaxation are widely studied in the context of these applications. In this study, we theoretically investigate the alignment dynamics of a rotational magnetic particle as an inverse process to Brownian relaxation. The selected external magnetic flux density ranges from 5 μ T to 5 T. We found that the viscous torque for arbitrary rotating particles with a history term due to the inertia and friction of the surrounding ambient water has a significant effect in strong magnetic fields (range 1–5 T). In this range, oscillatory behavior due to the inertial torque of the particle also occurs, and the stochastic Brownian torque diminishes. In contrast, for weak fields (range 5–50 μ T), the history term of the viscous torque and the inertial torque can be neglected, and the stochastic Brownian torque induced by random collisions of the surrounding fluid molecules becomes dominant. These results contribute to a better understanding of the molecular mechanisms of magnetic particle alignment in external magnetic fields and have important implications in a variety of biomedical applications.

Keywords: magnetic particle alignment rotational dynamics; viscous torque; stochastic Brownian torque; stochastic integro-differential equations; simulations



Citation: Krafcik, A.; Babinec, P.; Strbak, O.; Frollo, I. A Theoretical Analysis of Magnetic Particle Alignment in External Magnetic Fields Affected by Viscosity and Brownian Motion. *Appl. Sci.* **2021**, *11*, 9651. <https://doi.org/10.3390/app11209651>

Academic Editor: Kamil Gareev

Received: 27 September 2021

Accepted: 13 October 2021

Published: 15 October 2021

Publisher's Note: MDPI stays neutral with regard to jurisdictional claims in published maps and institutional affiliations.



Copyright: © 2021 by the authors. Licensee MDPI, Basel, Switzerland. This article is an open access article distributed under the terms and conditions of the Creative Commons Attribution (CC BY) license (<https://creativecommons.org/licenses/by/4.0/>).

1. Introduction

When subjected to an external magnetic field, a magnetic particle will respond with translational motion in the gradient magnetic field and its self-rotation, or rotation of its

magnetic moment, to the direction of the external magnetic field as it is applied in various cases of biomedical applications widely studied experimentally and theoretically [1–10]. These latter effects are simply denoted as magnetic alignment and are inverse processes to Brownian and Néel relaxation [11,12].

Both magnetic alignment and relaxation are important in, for example, magnetic particle contrast imaging and quantification in magnetic resonance and particle imaging [8,9,13–15], electromagnetic hyperthermia [6,7,16,17], theranostics [18–20], magnetorelaxometry [10,21,22], and navigation in the geomagnetic field [23–27]. Magnetic particle alignment at the nano- and micro-scale requires a complex approach for simulating a wide range of possible strengths of an acting external magnetic field. However, to our knowledge, such a study does not currently exist.

If we restrict only the particle rotating (as a whole with a magnetic moment) to the direction of an external homogeneous magnetic field, the particle experiences a magnetic torque that can be easily described analytically [28].

An object moving or rotating in a viscous ambient fluid experiences an action against its movement due to the internal friction of the ambient fluid. Such a fluid on the surface of the object moves with the object with the same velocity as its surface, i.e., it fulfills the no-slip boundary condition. The velocity of the layers of the fluid parallel to the object surface decreases with increasing distance between the layer and particle surface due to the internal friction of the fluid [29]. If the object is a sphere rotating about its axis with an arbitrary angular velocity, the torque felt by the sphere due to the internal friction of the fluid and its inertia adds an integral term for the whole history and development of angular acceleration to the quasi-steady viscous torque, as shown previously [30]. This integral history term is analogous to the Basset history force [31,32] (such a non-local Basset force was studied by our group recently as the correction of the magnetic particle separation dynamics in [5]). This term has its origin in the vortices of an ambient fluid around an arbitrary rotating sphere. The viscous torque is denoted as $\vec{T}_v(t)$, i.e., an “arbitrary viscous torque”.

Furthermore, when a spherical particle is sufficiently small, it experiences the stochastic effect of the Brownian motion of ambient fluid molecules [33], which depends on its temperature. This contribution to the overall torque is denoted as the $\vec{T}_B(t)$, i.e., a stochastic Brownian torque.

In most studies [34–36], the history acceleration term of the arbitrary viscous torque, inertia, and especially stochastic Brownian torques, are assumed to be negligible, and a simple viscous torque (a quasi-steady term, $\gamma\omega = 8\pi\eta R^3\omega$, for a sphere of radius R rotating with angular velocity ω in an ambient viscous fluid with dynamic viscosity η [37]) are considered, as in [17,25,33]. Alternatively, the thermal disturbance of magnetic alignment through the rotational diffusion model can be analyzed [38,39]. Particularly, the borderline from ballistic to diffusion behavior should be considered [40].

Therefore, in this study, our aim was to develop a complex model of the magnetic alignment of a single magnetic particle in an external homogeneous magnetic field. Originally, a quiescent ambient viscous fluid, together with consideration of the arbitrary viscous torque with the history acceleration term, as well as the stochastic Brownian torque for a defined temperature. The rotational movement of the sphere can then be modeled by a Langevin-like equation with a stochastic fluctuating torque due to random impulses from the many neighboring fluid molecules (similar to the Langevin equation in [41,42]), with a modified viscous torque through the use of the history term (see, for example, [43–45]).

The description of such a system is far from trivial. The stochastic term brings white noise to the model, which is mostly discontinuous and has infinite variations [46]. We consider not only a simple system of ordinary differential equations (ODEs) but also stochastic integro-differential equations (SIDEs), which do not possess a simple analytic or numerical solution. Recently, we showed in [5,47,48] how to approach a similar system of integro-differential equations (IDEs) containing a non-local Basset acceleration history term numerically, with a variable timestep order of one, quadrature scheme. However, the current situation is more complex because the stochastic term brings the additional

difficulty of solving the current system of SDEs with a similar method. Therefore, we use an approach arising from the simple finite difference method of Euler [49].

The computer source codes developed in this research are available as the Supplementary Materials.

2. Materials and Methods

2.1. Physical Model

If we consider a spherical magnetic particle with radius R , mass density ρ_p , and norm of magnetic moment μ_p , initially perpendicularly rotated to an external homogeneous magnetic field with flux density $\vec{B}_0 \equiv B_0 \vec{i}$, i.e., $\vec{\mu}_p(0) \equiv \mu_p \vec{j}$, located in a viscous ambient fluid with mass density ρ , dynamic viscosity η , and kinematic viscosity $\nu \equiv \eta/\rho$, then the rotational movement of the particle (alignment to the direction of the external magnetic field) can be described with a system of differential equations (DEs):

$$\vec{I}_p \cdot \frac{d\vec{\omega}(t)}{dt} = \vec{\mu}_p \times \vec{B}_0 + \vec{T}_v(t) + \vec{T}_B(t), \tag{1}$$

where \vec{I}_p is the moment of inertia tensor of the spherical particle, which for simple rotation about the particle axis reduces to the scalar $I_p = \frac{2}{5}m_p R^2$ and $\vec{\omega} \equiv \omega \vec{k}$ is the angular velocity of the rotational movement of the spherical particle. Unit vectors \vec{i}, \vec{j} , and \vec{k} form the basis of a Cartesian coordinate system. $m_p = V_p \rho_p$ is the weight of the magnetic particle and V_p is its volume. The first term on the right-hand side of Equation (1) is the magnetic torque exerted by the external homogeneous magnetic field \vec{B}_0 on the particle with magnetic moment $\vec{\mu}_p = \mu_p(\cos \varphi \vec{i} - \sin \varphi \vec{j})$. The second term in Equation (1) is the viscous torque of the viscous ambient fluid on the rotating spherical particle. The final term in Equation (1) is the random Brownian torque exerted on the spherical particle.

Due to the axial symmetry of the rotational movement of the spherical particle ($\vec{\omega} \parallel \vec{k}$), the system of DEs (1) becomes a scalar differential equation:

$$I_p \underbrace{\frac{d\omega(t)}{dt}}_{\text{inertial}} = \underbrace{\mu_p B_0 \sin \varphi}_{\text{magnetic}} + \underbrace{T_v(t)}_{\text{viscous}} + \underbrace{T_B(t)}_{\text{Brownian}}, \tag{2}$$

which together with:

$$\frac{d\varphi(t)}{dt} = -\omega(t), \tag{3}$$

and initial conditions:

$$\varphi(0) = \frac{\pi}{2} \text{ rad}, \quad \omega(0) = 0 \text{ rad/s}, \tag{4}$$

define the rotational alignment of the spherical particle with magnetic moment μ_p in the external homogeneous magnetic field with flux density B_0 and viscous fluid with thermodynamic temperature T .

The viscous torque $\vec{T}_v(t) = T_v(t)\vec{k}$ exerted on the spherical particle for arbitrary angular velocity $\omega(t)$ can be expressed according to [30]:

$$T_v(t) \equiv \underbrace{-\gamma \omega(t)}_{\text{quasi-steady}} - \underbrace{\frac{\gamma}{3\sqrt{\pi}} \int_{-\infty}^t K(t-\tau) \frac{d\omega(\tau)}{d\tau} d\tau}_{\text{history acceleration torque}}, \tag{5}$$

arbitrary viscous torque

where $\gamma \equiv 8\pi\eta R^3$ is the Stokes coefficient of the viscous torque and:

$$K(t - \tau) \equiv \frac{R}{\sqrt{\nu(t - \tau)}} - \sqrt{\pi} \exp\left(\frac{\nu(t - \tau)}{R^2}\right) \operatorname{erfc}\left(\frac{\sqrt{\nu(t - \tau)}}{R}\right) \tag{6}$$

is a kernel function. This brings a challenge to the solution of the system of DEs (2)–(3) with initial conditions (4), due to the history integral term in equation (5) over the whole evolution of the angular acceleration of the particle in time, known as the history acceleration torque.

Moreover, the fluctuating Brownian torque is a stochastic term generated with random impulses from the neighboring fluid molecules and its mathematical representation yields the properties of the Gaussian white noise phenomenon $W(t)$, i.e., in the first moment $\langle W(t) \rangle = 0$ (zero mean) and in the second $\langle W(t)W(t + \tau) \rangle = \delta(\tau)$ (uncorrelation) [41], where $\langle \dots \rangle$ represents an ensemble average and $\delta(\tau)$ is the Dirac delta function. The stochastic Brownian torque can then be expressed as:

$$T_B(t) \equiv \sqrt{2k_B T \gamma} W(t), \tag{7}$$

where k_B and T are the Boltzmann constant and thermodynamic temperature, respectively.

The studied problem is not only the system of ODEs but also the system of SODEs.

2.2. Solution

To solve the system of SODEs (2)–(7), we used the first-order integration method, generalizing the Euler method for stochastic differential equations (finite difference approach).

For memory integral integration in the arbitrary viscous torque evaluation of the acceleration torque, an order one quadrature scheme, similar to those presented in [50], is generally used. However, in contrast, we have used a different kernel function (6) arising from the definition of viscous torque equation (5). The integral occurring in this equation can be transcribed using integration by parts:

$$\int_{t_0}^t K(t - \tau) \frac{d\omega(\tau)}{d\tau} d\tau + K(t - t_0)\omega(t_0) = \frac{d}{dt} \int_{t_0}^t K(t - \tau)\omega(\tau) d\tau. \tag{8}$$

Now, we can divide the time span by the sequence of $n - 1$ constant timestep intervals $h = \tau_{i+1} - \tau_i$ for $i = 1$ to $n - 1$, where $\tau_1 = t_0$ and $\tau_n = t$, which gives:

$$\frac{d}{dt} \int_{t_0}^t K(t - \tau)\omega(\tau) d\tau = \frac{d}{dt} \sum_{i=1}^{n-1} \int_{\tau_i}^{\tau_{i+1}} K(t - \tau)\omega(\tau) d\tau \equiv \frac{d}{dt} \sum_{i=1}^{n-1} I_i(t). \tag{9}$$

If we now examine the simplest case, a linear approximation, the calculation leads to an order one quadrature scheme. By approximating $\omega(\tau)$ linearly in the interval $\tau \in [\tau_i, \tau_{i+1}]$:

$$\omega(\tau) = \omega(\tau_i) + \frac{\omega(\tau_{i+1}) - \omega(\tau_i)}{h} (\tau - \tau_i) + \mathcal{O}(h^2), \tag{10}$$

we obtain:

$$I_i(t) \equiv \int_{\tau_i}^{\tau_{i+1}} K(t - \tau)\omega(\tau) d\tau = \left[\omega(\tau_i) + \mathcal{O}(h^2) \right] \int_0^h K(t - \tau_i - \tau) d\tau + \frac{\omega(\tau_{i+1}) - \omega(\tau_i)}{h} \int_0^h \tau K(t - \tau_i - \tau) d\tau. \tag{11}$$

The integrals in Equation (11), with kernel function (6), can be computed analytically to yield:

$$I_i(t) \approx \omega(\tau_i) \sqrt{\pi} \frac{R^2}{\nu} \left[\exp \frac{\nu(t - \tau_i - \tau)}{R^2} \operatorname{erfc} \frac{\sqrt{\nu(t - \tau_i - \tau)}}{R} \right]_{\tau=0}^h + \frac{\omega(\tau_{i+1}) - \omega(\tau_i)}{h} \left[\frac{2R^3}{\nu^{3/2}} \sqrt{t - \tau_i - \tau} + \sqrt{\pi} \left(\frac{R^4}{\nu^2} + \frac{R^2}{\nu} \tau \right) \exp \frac{\nu(t - \tau_i - \tau)}{R^2} \operatorname{erfc} \frac{\sqrt{\nu(t - \tau_i - \tau)}}{R} \right]_{\tau=0}^h, \quad (12)$$

if higher orders of h , than the first, are omitted.

A method that considers the stochastic term (7) in the solution of stochastic differential equations (SDEs), using a finite difference approach was shown in [42] and also used in [33]. The approach utilizes a discrete sequence of random numbers W_i that mimics the properties of $W(t)$ and is stationary with zero mean, as well as having to fulfill $\langle W(t)^2 \rangle = 1$ for each value of t , which in a discrete sequence sense means that $\langle (W_i \Delta t)^2 \rangle / \Delta t = 1$, i.e., the W_i has variance $1 / \Delta t$. Furthermore, because $W(t)$ is uncorrelated, we assume W_i and W_j to be independent for $i \neq j$, i.e., we use a sequence of uncorrelated random numbers with zero mean and variance $1 / \Delta t$. The realization of a such sequence is as simple as:

$$W_i = \frac{w_i}{\sqrt{\Delta t}} \equiv \frac{w_i}{\sqrt{h}}, \quad (13)$$

where w_i is a Gaussian random number with zero mean and unit variance. For the timestep Δt , we used the standard notation h , as used above. The discrete stochastic Brownian torque value in the i -th timestep is then given by:

$$T_{B,i} \equiv \sqrt{\frac{2k_B T \gamma}{h}} w_i. \quad (14)$$

In a discrete sense, the solution for the n -th step of the angle and angular velocity can be expressed using the finite difference method as:

$$\varphi_n = \frac{2I_p + \gamma h}{I_p + \gamma h} \varphi_{n-1} - \frac{I_p}{I_p + \gamma h} \varphi_{n-2} - \frac{\mu_p B_0 h^2}{I_p + \gamma h} \sin \varphi_{n-1} - \frac{h^2}{I_p + \gamma h} T_{acc,n} - \frac{\sqrt{2k_B T \gamma} h^{\frac{3}{2}}}{I_p + \gamma h} w_n, \quad (15)$$

$$\omega_n = -\frac{\varphi_n - \varphi_{n-1}}{h}, \quad (16)$$

where the history acceleration torque fulfills in the n -th step:

$$T_{acc,n} = -\frac{\gamma}{3\sqrt{\pi}} \left[-K(t - t_0) \omega(t_0) + \frac{S_n - S_{n-1}}{h} \right] \quad (17)$$

with $S_n \equiv \sum_{i=1}^{n-1} I_i(t)$ and S_{n-1} is the S_n from the previous step.

3. Results and Discussion

We simulated the rotational alignment of a spherical MyOne 1.0 μm microparticle [ThermoFischer Scientific, Waltham, MA USA, DynabeadsTM, MyOneTM, available online: <https://www.thermofisher.com/order/catalog/product/65012?SID=srch-srp-65012> (accessed on 31 May 2018)] in an external homogeneous magnetic field and water as an ambient viscous fluid, with its parameters shown in Table 1.

Table 1. Values of parameters used in simulations.

Parameter	Symbol	Value	Unit
Finite timestep	h	10^{-8}	s
Boltzmann constant	k_B	1.3807×10^{-23}	JK^{-1}
Thermodynamic temperature	T	293.15	K
Fluid ^a dynamic viscosity	η	10^{-3}	Pa s
Fluid mass density	ρ	1000	kg m^{-3}
Fluid kinematic viscosity	ν	η/ρ	$\text{m}^2 \text{s}^{-1}$
Magnetic flux density norm	B_0	$5 \times 10^{-6}, \dots, 5$	T
Particle ^b diameter	$2R$	10^{-6}	m
Particle mass density	ρ_p	1792	kg m^{-3}
Particle volume	V_p	$\frac{4}{3}\pi R^3$	m^3
Particle weight	m_p	$V_p \rho_p$	kg
Particle moment of inertia	I_p	$\frac{2}{5}m_p R^2$	kg m^2
Particle saturation magnetization	M_{sp}	43.0×10^3	A m^{-1}
Particle magnetic moment ^c	μ_p	2.25×10^{-14}	A m^2
Stokes coefficient	γ	$8\pi\eta R^3$	$\text{kg m}^2 \text{s}^{-1}$

^a Water as an ambient fluid. ^b Parameters of commercially available magnetic particle MyOne 1 μm (ThermoFischer Scientific, Waltham, MA USA, DynabeadsTM, MyOneTM). ^c Magnetic moment calculated as $\mu_p = M_{sp}V_p$.

3.1. Comparison of Models

Simulations were performed for four different combinations of the considered effects and these were denoted as four different models, as shown in Table 2, where the abbreviated notation of each model is explicitly defined. The magnitude of the external homogeneous magnetic flux density field B_0 was used for each model with a scale of 5 μT to 5 T. The obtained results are shown in Figure 1.

Table 2. Model notation with specified torques involved in simulations.

No.	Torques Involved	Notation
(i)	inertial, magnetic, quasi-steady viscous, stochastic Brownian	SDE ^a
(ii)	inertial, magnetic, arbitrary viscous, stochastic Brownian	SIDE ^b
(iii)	inertial, magnetic, quasi-steady viscous, no stochastic Brownian	ODE ^c
(iv)	inertial, magnetic, arbitrary viscous, no stochastic Brownian	IDE ^d

^a Stochastic differential equations. ^b Stochastic integro-differential equations. ^c Ordinary differential equations.

^d Integro-differential equations.

From the solutions shown in Figure 1, a strong dependence for the speed of magnetic particle alignment on the magnitude of the magnetic flux density acting on the particle can be seen. For strong fields, the process of magnetic alignment is rapid and slowed down with decreasing B_0 .

Strong magnetic fields acting on the magnetic particles in water as the ambient fluid at a temperature of 293.15 K cause rapid magnetic particle alignment with a characteristic timescale of the order of microseconds. In weaker fields, this time rises significantly by approximately one order of magnitude with each decreasing order of magnitude of the external magnetic flux density field.

It can be seen that the time evolution of the angle and angular velocity for the strongest B_0 field and for all modeled combinations of considered effects exhibit characteristic oscillations and nearly exponential decaying behavior. With a decrease in the magnetic flux density B_0 field, the oscillations disappear even though the almost exponential decaying behavior persists.

For the SDE and SIDE models, weakening the external B_0 fields stochastic Brownian torque results in a random pattern in the evolution of the angle and angular velocity with the appearance of stochastic jumps, firstly for $\omega(t)$ and also for $\varphi(t)$ for the weakest B_0 fields (see Figure 1e–g).

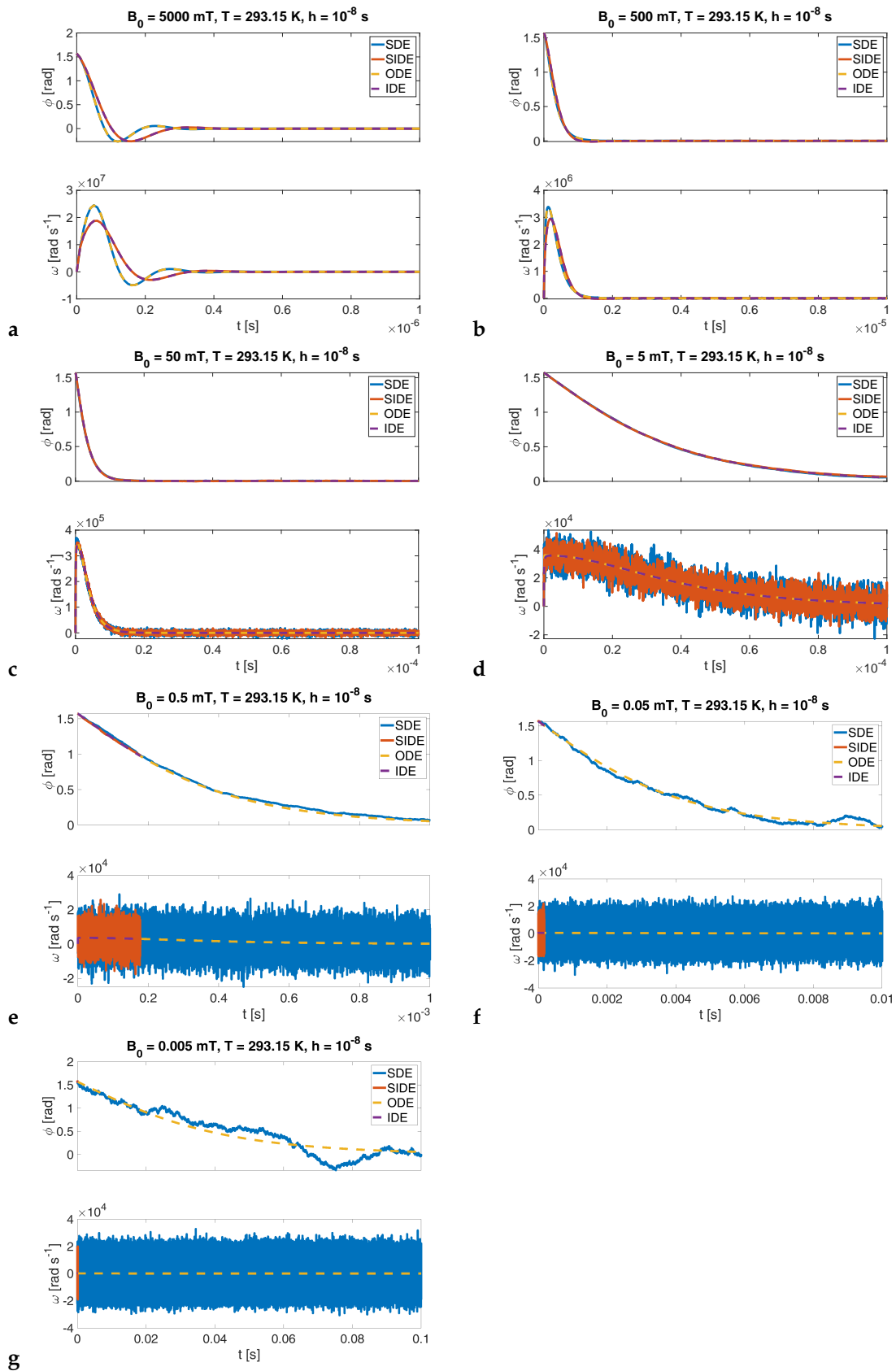


Figure 1. Comparison of all considered models of rotational magnetic particle alignment for B_0 from 5 T down to 5 μ T in panels (a–g), respectively. In the weakest B_0 fields (panels (e–g)), premature stopping of simulations for SIDE and IDE models occurs due to a math range error in the numerical evaluation of the $f(x) = \exp(x)$ function occurring in the kernel function (6).

3.2. Strong B_0 Field Limit Case

For the strong magnetic flux density field limit case, the time evolution of $\varphi(t)$ and $\omega(t)$ in Figure 1a,b is shown, and it is clear that the viscous history acceleration torque as part of the arbitrary viscous torque starts to have a significant effect. The involvement of the history acceleration torque term in the SIDE and IDE models results in a reduction in the amplitude of the angle and angular velocity at the early stage of alignment in comparison with the SDE and ODE models. For $B_0 = 5$ T (Figure 1a), this correction of the $\varphi(t)$ amplitude caused by the history acceleration torque is a few percent. The correction of the $\omega(t)$ amplitude is $>10\%$. Furthermore, the stochastic Brownian torque effect is minimal and, for the temperature considered, can be neglected.

For a better illustration of the significance of each torque in the strong B_0 field limit for the complex SIDE model (i.e., inertial, magnetic, arbitrary viscous, and stochastic Brownian torques) during the whole time evolution, see Figure 2.

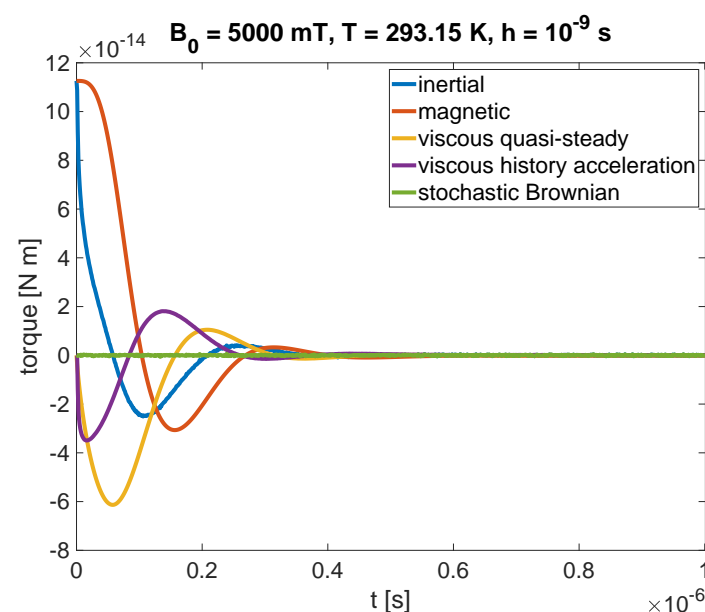


Figure 2. Time evolution of each kind of torque for the strong B_0 field limit generated with the SIDE model. For comparison, see the time evolution of $\varphi(t)$ and $\omega(t)$ in Figure 1a.

The observed oscillatory character of the $\varphi(t)$ and $\omega(t)$ time evolution in the strongest B_0 field has its origin in the involvement of the inertial torque in the description of the models. In contrast, its diminishment, for instance, at a low Reynolds number limit, results in a loss of this oscillatory behavior.

As much as the usual inertia contribution, the non-local Basset force is usually negligible at the macroscopic observation time scales considered in standard tracking experiments, but its effects have been shown to be prominent at short time-scales in [51,52]. This finding is an analogue to the behavior of our studied system with the non-Basset kernel of the history acceleration torque for arbitrary rotating sphere.

3.3. Weak B_0 Field Limit Case

The simulations for the SIDE and IDE models and for weaker B_0 fields were prematurely stopped due to excessively high values of exponents in the expression for the kernel function for the arbitrary viscous torque (history acceleration torque). Therefore, in the weakest B_0 fields, we only focused on the models without the history acceleration torque. In this weak B_0 field limit case, Figure 1f,g, the stochastic Brownian torque effect rises and starts to dominate. In contrast, even the viscous history acceleration torque (part of the arbitrary viscous torque) is numerically unreachable; its effect is minimal and can therefore be neglected.

The manifestation of stochastic behavior for the time evolution of angle $\varphi(t)$ is only visible for the weakest magnetic flux density fields. Even for the time evolution of the angular velocity $\omega(t)$, it occurs for the medium magnitudes of the magnetic field. The stochasticity of $\varphi(t)$ will also be visible for the same values of B_0 as for the stochastic behavior of $\omega(t)$ in the case of omitting the inertial torque from the models (low Reynolds number limit, not shown here). This discrepancy only disappears in the case of times significantly longer than the inertial time $\tau_{\text{inertial}} \equiv I_p/\gamma = 0.03 \mu\text{s}$, when both the time evolution of the angle for models with the inertial torque and without it are jagged because the microscopic details are not resolvable. Otherwise, the time evolution of the angle for the model with the inertial torque is smoothed [42].

The zero mean and uncorrelation of stochastic Brownian impulses to the magnetic particle are clearly visible in the averaged time evolution of $\varphi(t)$ for an ensemble of $N = 1000$ samples of rotational magnetic particle alignment, as shown in Figure 3a for the SDE model, meaning that the evolution replicates the time dependence of $\varphi(t)$ of the single ODE model. Furthermore, its region of variance, defined with lines of mean \pm std, does not change with the size of the finite timestep h (see Figure 3b).

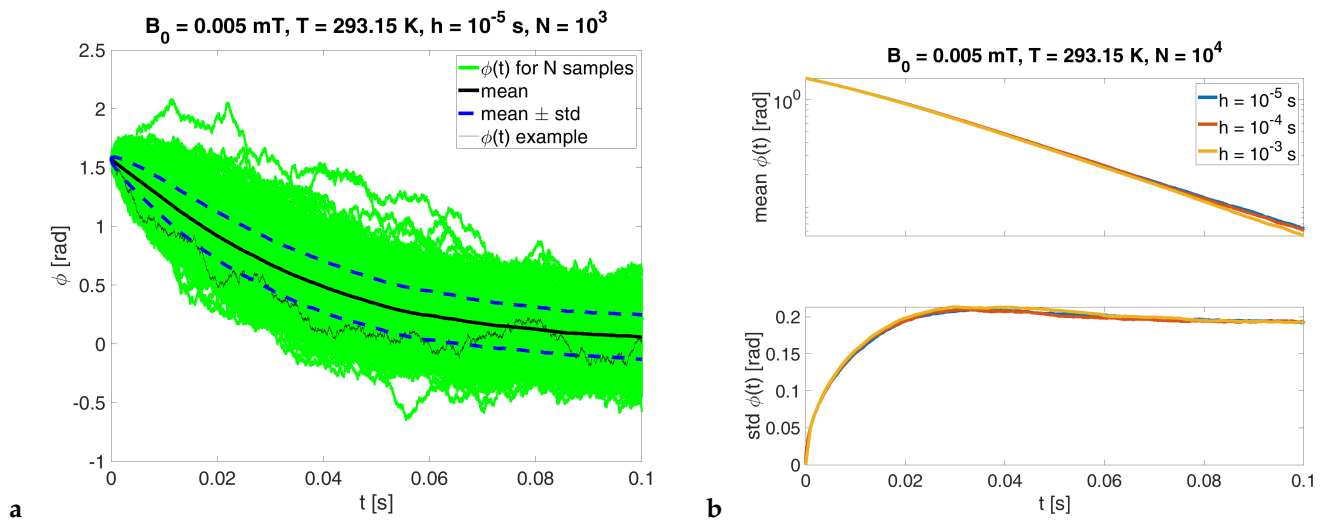


Figure 3. (a) Time evolution of $\varphi(t)$ for $N = 10^3$ samples of the SDE model, i.e., inertial, magnetic, quasi-steady viscous, and stochastic Brownian torques in the weak B_0 field limit (timestep $h = 10^{-5}$ s). (b) Comparison of time evolution of mean and std values of $\varphi(t)$ averaged over $N = 10^4$ samples of the SDE model for different finite timesteps h .

The stochastic Brownian torque term contribution to the overall dynamics of magnetic particle alignment increases with the weakening external magnetic flux density field B_0 , as discussed. This contribution will be even more visible for an increased thermodynamic temperature of the ambient fluid, while the stochastic Brownian torque depends on the square root of the thermodynamic temperature, Equation (7).

3.4. Characteristic Time of Magnetic Particle Alignment

The time evolution of $\varphi(t)$ for the simplest model, the ODE model, involving the inertial, magnetic, quasi-steady viscous, and no stochastic Brownian torques, was used as the input data for the least-square minimization fit using a fitting function:

$$\varphi(t) = \frac{\pi}{2} \exp\left(-\frac{t}{\tau_{\text{char}}}\right) \tag{18}$$

with the founded parameter τ_{char} for each B_0 . The obtained fits with estimated values of parameter τ_{char} are shown in Figure 4a–g. This parameter τ_{char} has the meaning of time t when the angle $\varphi(t)$ reduces to the value of $\frac{\pi}{2e}$ and, therefore, can be denoted as the characteristic time of magnetic particle alignment. The obtained fits from simulations are

in good agreement for the whole range of concerned B_0 , except for its strong limit case ($B_0 = 5000$ mT case in Figure 4g).

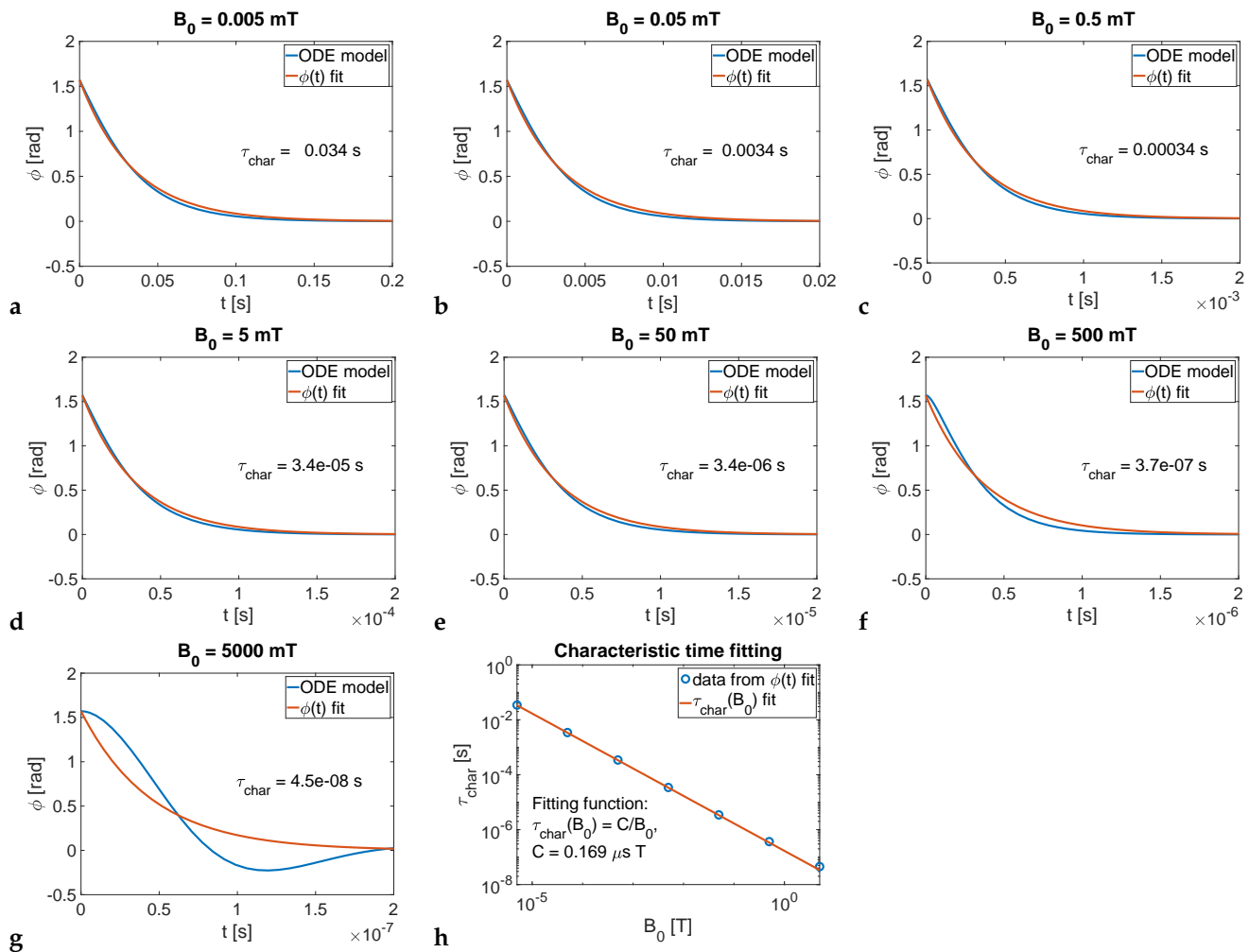


Figure 4. Least-square minimization fit of time evolution $\phi(t)$ for the simplest ODE model using function (18) and obtained estimates of characteristic time of magnetic particle alignment for each value of B_0 in the range from $5 \mu\text{T}$ to 5T shown in panels (a–g), respectively; and the (h) least-square minimization fit of the characteristic time dependence on magnetic flux density norm $\tau_{\text{char}}(B_0)$ using Equation (19).

The estimated values of τ_{char} for each B_0 were further used to find the expression of their dependence. The following fitting function was used:

$$\tau_{\text{char}}(B_0) = \frac{C}{B_0}. \tag{19}$$

Parameter C was found from the least-square minimization fit with the value $C = 0.169 \mu\text{s T}$ (see Figure 4h).

3.5. Limitations

To summarize, a complex theoretical model of rotational magnetic particle alignment for external homogeneous magnetic flux density magnitudes B_0 from $5 \mu\text{T}$ to 5T in water as an ambient viscous fluid at room temperature has been presented. It has been shown that the significance of the arbitrary viscous torque history term increases in the strong B_0 limit. In contrast, in the weak B_0 field limit, it diminishes, and the stochastic Brownian torque effect starts to manifest. In addition, the characteristic time of magnetic particle alignment for the entire scale of B_0 magnitudes has been estimated.

The presented models bring several simplifications and limitations to the studied system, as discussed below.

The weakening of the B_0 field causes prolongation of the time needed for rotational magnetic particle alignment. This implies increasing the argument of the exponential function in the kernel function definition with the lowering of B_0 , which is limited in the numerical realization of the $f(x) = \exp(x)$ function. The solution of this problem is simple. The effect of the history term in the weak field is minimal and diminishes, so we do not need to solve the whole problem (SIDE model) in the weak B_0 limit and can neglect it and focus only on the solution of the SDE model.

Due to the non-locality of the history acceleration torque, the stochastic Brownian torque should be not mathematically represented as a Gaussian white random process in Langevin theory [53], but instead as a “colored” one [45]. However, the correlation in the time of the random process, due to the neglect of the history term in the weak B_0 limit, when the stochastic Brownian torque effect manifests, diminishes. Therefore, the stochastic Brownian torque can be considered as a zero-mean uncorrelated random process. In reality, the system memory can affect the “color” of the Brownian random process [45,51]. The external forces can also affect the memory of the system and thermal force as it was discussed, for example in [54–58]. A solution of the studied problem in this way is still missing.

The particle magnetic moment of the considered models comes from the assumption of its constant value, which in reality is not fulfilled, while the used particle is paramagnetic. Therefore, the involvement of a magnetic moment saturation process in future models will be convenient.

Supplementary Materials: The following is available online at <https://www.mdpi.com/article/10.3390/app11209651/s1>, Computer Source Codes S1: particle-alignment-models.py and particle-alignment-side-torques.py (developed in PYTHON 3.8.3) zipped in a single file.

Author Contributions: Conceptualization, A.K. and O.S.; methodology, A.K. and P.B.; software, A.K.; validation, A.K.; formal analysis, A.K.; investigation, A.K. and P.B.; resources, I.F. and O.S.; data curation, A.K.; writing—original draft preparation, A.K.; writing—review & editing, P.B. and O.S.; visualization, A.K.; supervision, P.B.; project administration, I.F. and O.S.; funding acquisition, I.F. and O.S. All authors have read and agreed to the published version of the manuscript.

Funding: This research was funded by the Slovak Research and Development Agency (APVV-19-0032), by the Slovak Scientific Grant Agency (VEGA 2/0003/20), and by the Ministry of Health of the Slovak Republic (2018/11-UKMT-7).

Institutional Review Board Statement: Not applicable.

Informed Consent Statement: Not applicable.

Data Availability Statement: Data supporting our results are available as the computer source codes with details specified in the Supplementary Materials section.

Conflicts of Interest: The authors declare no conflict of interest. The funders had no role in the design of the study; in the collection, analyses, or interpretation of data; in the writing of the manuscript, or in the decision to publish the results.

Abbreviations

The following abbreviations are used in this manuscript:

DEs	System of differential equations
IDEs	System of integro-differential equations
MPI	Magnetic particle imaging
MRI	Magnetic resonance imaging
ODEs	System of ordinary differential equations
SDEs	System of stochastic differential equations
SIDEs	System of stochastic integro-differential equations

References

1. Dames, P.; Gleich, B.; Flemmer, A.; Hajek, K.; Seidl, N.; Wiekhorst, F.; Eberbeck, D.; Bittmann, I.; Bergemann, C.; Weyh, T.; et al. Targeted delivery of magnetic aerosol droplets to the lung. *Nat. Nanotechnol.* **2007**, *2*, 495–499. [[CrossRef](#)] [[PubMed](#)]
2. Krafcik, A.; Babinec, P.; Frollo, I. Computational analysis of magnetic field induced deposition of magnetic particles in lung alveolus in comparison to deposition produced with viscous drag and gravitational force. *J. Magn. Magn. Mater.* **2015**, *380*, 46–53. [[CrossRef](#)]
3. Surendran, A.; Zhou, R.; Lin, Y. Microfluidic Devices for Magnetic Separation of Biological Particles: A Review. *J. Med. Devices Trans. ASME* **2021**, *15*, 024001. [[CrossRef](#)]
4. Babinec, P.; Krafcik, A.; Babincova, M.; Rosenecker, J. Dynamics of magnetic particles in cylindrical Halbach array: Implications for magnetic cell separation and drug targeting. *Med. Biol. Eng. Comput.* **2010**, *48*, 745–753. [[CrossRef](#)]
5. Krafcik, A.; Babinec, P.; Babincova, M.; Frollo, I. High gradient magnetic separation with involved Basset history force: Configuration with single axial wire. *Powder Technol.* **2019**, *347*, 50–58. [[CrossRef](#)]
6. Perigo, E.A.; Hemery, G.; Sandre, O.; Ortega, D.; Garaio, E.; Plazaola, F.; Teran, F.J. Fundamentals and advances in magnetic hyperthermia. *Appl. Phys. Rev.* **2015**, *2*, 041302. [[CrossRef](#)]
7. Babincova, N.; Sourivong, P.; Babinec, P.; Bergemann, C.; Babincova, M.; Durdik, S. Applications of magnetoliposomes with encapsulated doxorubicin for integrated chemotherapy and hyperthermia of rat C6 glioma. *Z. Naturforsch. Sect. C J. Biosci.* **2018**, *73*, 265–271. [[CrossRef](#)]
8. Saritas, E.; Goodwill, P.; Croft, L.; Konkle, J.; Lu, K.; Zheng, B.; Conolly, S. Magnetic particle imaging (MPI) for NMR and MRI researchers. *J. Magn. Reson.* **2013**, *229*, 116–126. [[CrossRef](#)]
9. Strbak, O.; Antal, I.; Khmara, I.; Koneracka, M.; Kubovcikova, M.; Zavisova, V.; Molcan, M.; Jurikova, A.; Hnilicova, P.; Gombos, J.; et al. Influence of dextran molecular weight on the physical properties of magnetic nanoparticles for hyperthermia and MRI applications. *Nanomaterials* **2020**, *10*, 2468. [[CrossRef](#)]
10. Strbak, O.; Balejckikova, L.; Kmetova, M.; Gombos, J.; Kovac, J.; Dobrota, D.; Kopcansky, P. Longitudinal and transverse relaxivity analysis of native ferritin and magnetoferritin at 7 T MRI. *Int. J. Mol. Sci.* **2021**, *22*, 8487. [[CrossRef](#)]
11. Koksharov, Y.A. Magnetism of Nanoparticles: Effects of Size, Shape, and Interactions. In *Magnetic Nanoparticles*; Gubin, S.P., Ed.; John Wiley & Sons, Ltd.: Weinheim, Germany, 2009; Chapter 6, pp. 197–254. [[CrossRef](#)]
12. Dieckhoff, J.; Eberbeck, D.; Schilling, M.; Ludwig, F. Magnetic-field dependence of Brownian and Néel relaxation times. *J. Appl. Phys.* **2016**, *119*, 043903. [[CrossRef](#)]
13. Croft, L.; Goodwill, P.; Ferguson, M.; Krishnan, K.; Conolly, S. Relaxation in x-space magnetic particle imaging. *Springer Proc. Phys.* **2012**, *140*, 149–153. [[CrossRef](#)]
14. Estelrich, J.; Sanchez-Martín, M.; Busquets, M. Nanoparticles in magnetic resonance imaging: From simple to dual contrast agents. *Int. J. Nanomed.* **2015**, *10*, 1727–1741. [[CrossRef](#)]
15. Paysen, H.; Loewa, N.; Weber, K.; Kosch, O.; Wells, J.; Schaeffter, T.; Wiekhorst, F. Imaging and quantification of magnetic nanoparticles: Comparison of magnetic resonance imaging and magnetic particle imaging. *J. Magn. Magn. Mater.* **2019**, *475*, 382–388. [[CrossRef](#)]
16. Nishimoto, K.; Ota, S.; Shi, G.; Takeda, R.; Trisnanto, S.; Yamada, T.; Takemura, Y. High intrinsic loss power of multicore magnetic nanoparticles with blood-pooling property for hyperthermia. *AIP Adv.* **2019**, *9*, 035347. [[CrossRef](#)]
17. Manzin, A.; Ferrero, R.; Vicentini, M. From Micromagnetic to In Silico Modeling of Magnetic Nanodisks for Hyperthermia Applications. *Adv. Theory Simul.* **2021**, *4*, 2100013. [[CrossRef](#)]
18. Chandrasekharan, P.; Tay, Z.; Hensley, D.; Zhou, X.; Fung, B.; Colson, C.; Lu, Y.; Fellows, B.; Huynh, Q.; Saayujya, C.; et al. Using magnetic particle imaging systems to localize and guide magnetic hyperthermia treatment: Tracers, hardware, and future medical applications. *Theranostics* **2020**, *10*, 2965–2981. [[CrossRef](#)] [[PubMed](#)]
19. Gauger, A.; Hershberger, K.; Bronstein, L. Theranostics Based on Magnetic Nanoparticles and Polymers: Intelligent Design for Efficient Diagnostics and Therapy. *Front. Chem.* **2020**, *8*, 561. [[CrossRef](#)]
20. Hensley, D.; Tay, Z.; Dhavalikar, R.; Zheng, B.; Goodwill, P.; Rinaldi, C.; Conolly, S. Combining magnetic particle imaging and magnetic fluid hyperthermia in a theranostic platform. *Phys. Med. Biol.* **2017**, *62*, 3483–3500. [[CrossRef](#)]
21. Lange, J.; Kotitz, R.; Haller, A.; Trahms, L.; Semmler, W.; Weitschies, W. Magnetorelaxometry—A new binding specific detection method based on magnetic nanoparticles. *J. Magn. Magn. Mater.* **2002**, *252*, 381–383. [[CrossRef](#)]
22. Jaufenthaler, A.; Schultze, V.; Scholtes, T.; Schmidt, C.; Handler, M.; Stolz, R.; Baumgarten, D. OPM magnetorelaxometry in the presence of a DC bias field. *EPJ Quantum Technol.* **2020**, *7*, 12. [[CrossRef](#)]
23. Smith, M.; Sheehan, P.; Perry, L.; O'Connor, K.; Csonka, L.; Applegate, B.; Whitman, L. Quantifying the magnetic advantage in magnetotaxis. *Biophys. J.* **2006**, *91*, 1098–1107. [[CrossRef](#)] [[PubMed](#)]
24. Bennet, M.A.; Eder, S.H.K. Magnetoreception and Magnetotaxis. In *Iron Oxides: From Nature to Applications*; Faivre, D., Ed.; John Wiley & Sons, Ltd.: Weinheim, Germany, 2016; Chapter 22, pp. 567–590. [[CrossRef](#)]
25. Satyanarayana, S.; Padmaprahada, S.; Chitradurga, R.; Bhattacharya, S. Orientational dynamics of magnetotactic bacteria in Earth's magnetic field—A simulation study. *J. Biol. Phys.* **2021**, *47*, 79–93. [[CrossRef](#)]
26. Erglis, K.; Wen, Q.; Ose, V.; Zeltins, A.; Sharipo, A.; Janmey, P.; Cebers, A. Dynamics of magnetotactic bacteria in a rotating magnetic field. *Biophys. J.* **2007**, *93*, 1402–1412. [[CrossRef](#)]
27. Lohmann, K. QA: Animal behaviour: Magnetic-field perception. *Nature* **2010**, *464*, 1140–1142. [[CrossRef](#)]

28. Jackson, J.D. *Classical Electrodynamics*, 3rd ed.; Wiley: New York, NY, USA, 1999.
29. Box, F.; Thompson, A.; Mullin, T. Torsional oscillations of a sphere in a Stokes flow. *Exp. Fluids* **2015**, *56*, 209. [[CrossRef](#)]
30. Lei, U.; Yang, C.; Wu, K. Viscous torque on a sphere under arbitrary rotation. *Appl. Phys. Lett.* **2006**, *89*, 181908. [[CrossRef](#)]
31. Basset, A.B.; Strutt, J.W., III. On the motion of a sphere in a viscous liquid. *Philos. Trans. R. Soc. A* **1888**, *179*, 43–63. [[CrossRef](#)]
32. Premrata, A.; Wei, H.H. Atypical non-Basset particle dynamics due to hydrodynamic slip. *Phys. Fluids* **2020**, *32*, 097109. [[CrossRef](#)]
33. Romodina, M.; Lyubin, E.; Fedyanin, A. Detection of Brownian Torque in a Magnetically-Driven Rotating Microsystem. *Sci. Rep.* **2016**, *6*, 21212. [[CrossRef](#)] [[PubMed](#)]
34. Helgesen, G.; Pieranski, P.; Skjeltorp, A. Nonlinear phenomena in systems of magnetic holes. *Phys. Rev. Lett.* **1990**, *64*, 1425–1428. [[CrossRef](#)]
35. McNaughton, B.; Agayan, R.; Wang, J.; Kopelman, R. Physicochemical microparticle sensors based on nonlinear magnetic oscillations. *Sens. Actuators B Chem.* **2007**, *121*, 330–340. [[CrossRef](#)]
36. Tierno, P.; Claret, J.; Sagues, F.; Cabers, A. Overdamped dynamics of paramagnetic ellipsoids in a precessing magnetic field. *Phys. Rev. E Stat. Nonlinear Soft Matter Phys.* **2009**, *79*, 021501. [[CrossRef](#)]
37. Lamb, H. *Hydrodynamics*, 6th ed.; Cambridge University Press: Cambridge, UK, 1932.
38. Yamaguchi, M.; Ozawa, S.; Yamamoto, I. Rotational diffusion model of magnetic alignment. *Jpn. J. Appl. Phys.* **2009**, *48*, 063001. [[CrossRef](#)]
39. Yamaguchi, M.; Ozawa, S.; Yamamoto, I.; Kimura, T. Characterization of three-dimensional magnetic alignment for magnetically biaxial particles. *Jpn. J. Appl. Phys.* **2013**, *52*, 013003. [[CrossRef](#)]
40. Ilyin, V.; Procaccia, I.; Zagorodny, A. Stochastic processes crossing from ballistic to fractional diffusion with memory: Exact results. *Condens. Matter Phys.* **2010**, *13*, 23001–23008. [[CrossRef](#)]
41. Jones, R.B. *Rotational Diffusion in Dispersive Media*; Centre of Excellence for Advanced Materials and Structures: Warsaw, Poland, 2003.
42. Volpe, G.; Volpe, G. Simulation of a Brownian particle in an optical trap. *Am. J. Phys.* **2013**, *81*, 224–230. [[CrossRef](#)]
43. Tothova, J.; Vasziouva, G.; Glod, L.; Lisy, V. Langevin theory of anomalous Brownian motion made simple. *Eur. J. Phys.* **2011**, *32*, 645–655. [[CrossRef](#)]
44. Tothova, J.; Vasziouva, G.; Glod, L.; Lisy, V. A note on ‘Langevin theory of anomalous Brownian motion made simple’. *Eur. J. Phys.* **2011**, *32*, L04. [[CrossRef](#)]
45. Tothova, J.; Lisy, V. Generalized Langevin theory of the Brownian motion and the dynamics of polymers in solution. *Acta Phys. Slovaca* **2015**, *65*, 1–64.
46. Øksendal, B. *Stochastic Differential Equations: An Introduction with Applications (Universitext)*, 6th ed.; Springer: Berlin, Germany, 2014.
47. Krafcik, A.; Babinec, P.; Frollo, I. Stokes versus Basset: Comparison of forces governing motion of small bodies with high acceleration. *Eur. J. Phys.* **2018**, *39*, 035805. [[CrossRef](#)]
48. Krafcik, A.; Babinec, P.; Babincova, M.; Frollo, I. Importance of Basset history force for the description of magnetically driven motion of magnetic particles in air. *Meas. Sci. Rev.* **2020**, *20*, 50–58. [[CrossRef](#)]
49. Butcher, J.C. *Numerical Methods for Ordinary Differential Equations*; John Wiley & Sons, Ltd.: New York, NY, USA, 2003; [[CrossRef](#)]
50. Daitche, A. Advection of inertial particles in the presence of the history force: Higher order numerical schemes. *J. Comput. Phys.* **2013**, *254*, 93–106. [[CrossRef](#)]
51. Franosch, T.; Grimm, M.; Belushkin, M.; Mor, F.; Foffi, G.; Forro, L.; Jeney, S. Resonances arising from hydrodynamic memory in Brownian motion. *Nature* **2011**, *478*, 85–88. [[CrossRef](#)] [[PubMed](#)]
52. Huang, R.; Chavez, I.; Taute, K.; Lukic, B.; Jeney, S.; Raizen, M.; Florin, E.L. Direct observation of the full transition from ballistic to diffusive Brownian motion in a liquid. *Nat. Phys.* **2011**, *7*, 576–580. [[CrossRef](#)]
53. Zwanzig, R. *Nonequilibrium Statistical Mechanics*; Oxford University Press: New York, NY, USA, 2001.
54. Lisy, V.; Tothova, J. Generalized Langevin equation and the fluctuation-dissipation theorem for particle-bath systems in a harmonic field. *Results Phys.* **2019**, *12*, 1212–1213. [[CrossRef](#)]
55. Lisy, V.; Tothova, J. Brownian motion of charged particles in a bath responding to an external magnetic field. *Acta Phys. Pol. A* **2020**, *137*, 657–659. [[CrossRef](#)]
56. Tothova, J.; Soltys, A.; Lisy, V. Brownian motion in a bath responding to external electric fields. *J. Mol. Liq.* **2020**, *317*, 113920. [[CrossRef](#)]
57. Tothova, J.; Lisy, V. Brownian motion in a gas of charged particles under the influence of a magnetic field. *Phys. A Stat. Mech. Appl.* **2020**, *559*, 125110. [[CrossRef](#)]
58. Tothova, J.; Lisy, V. Brownian motion in a bath affected by an external harmonic potential. *Phys. Lett. Sect. A Gen. At. Solid. State Phys.* **2021**, *395*, 127220. [[CrossRef](#)]